Available online at www.sciencedirect.com

ScienceDirect

Ceramics International 40 (2014) 347–355

CERAMICS INTERNATIONAL

www.elsevier.com/locate/ceramint

The influence of laser treatment on thermal shock resistance of plasma-sprayed nanostructured yttria stabilized zirconia thermal barrier coatings

Reza Ghasemi*, Reza Shoja-Razavi, Reza Mozafarinia, Hossein Jamali

[a]*Department of Materials Engineering, Malek-Ashtar University of Technology, Shahinshahr, Isfahan, Iran*

Received 19 May 2013; received in revised form 2 June 2013; accepted 4 June 2013
Available online 15 June 2013

Abstract

The main goal of this paper was to evaluate the effects of laser glazing on the microstructure and thermal shock resistance of nanostructured thermal barrier coatings (TBCs). To this end, nanostructured yttria stabilized zirconia (YSZ) top coat and NiCrAlY bond coat were deposited on Inconel 738LC substrate by air plasma spraying (APS). The Nd:YAG pulsed laser was used for laser treatment of top coat surface. The thermal shock behavior of plasma-sprayed and laser-glazed coatings was investigated by quenching the samples in cold water from 1000 °C. The microstructure and phase composition of the coatings were characterized by scanning electron microscopy (SEM) and X-ray diffractometry (XRD). Energy dispersive spectroscopy (EDS) was used to analyze the interface diffusion behavior of the bond coat elements. The results of SEM revealed that the laser glazing process reduced the surface roughness, eliminated the porosity of the surface and produced network cracks perpendicular to the surface. XRD results also indicated that both as-sprayed and laser glazed coatings consisted of non-transformable (T′) phase. Thermal shock test results showed that the lifetimes of the plasma-sprayed TBCs were almost doubled by laser glazing. Continuous network of segmented cracks perpendicular to the surface produced by laser glazing improved the strain accommodation and recognized it as the main enhancement mechanism for TBC life extension.

Keywords: C. Thermal shock resistance; Microstructure; Laser glazing; Thermal barrier coating

1. Introduction

Thermal barrier coatings are highly advanced material systems usually applied to metallic surface, such as gas turbine engines which operate at elevated temperatures [1–3]. The TBC system consists of a ceramic top coat, a metallic bond coat, and a superalloy substrate [4,5]. The ceramic top coat is typically composed of yttria stabilized zirconia,which is desirable for ensuring low thermal conduction and high thermal expansion coefficient while remaining stable at oxidizing and combustion atmospheres, which closely match those of the substrate [6,7]. The bond coat consists of MCrAlY, where M is a metal such as Co and/or Ni. The bond coat layer generally ensures the adherence between the ceramic top coat and the substrate while improving the oxidation resistance of the underlying substrate alloy [8,9]. A thermally grown oxide (TGO) is formed at the interface between the bond coat and ceramic top coat due to high temperature oxidation of the bond coat [10,11].

Several techniques have been developed for the deposition of TBC, including plasma spraying, electron beam physical vapor deposition (EB-PVD) [12], chemical vapor deposition (CVD) [13], suspension plasma spraying (SPS) [14], solution precursor plasma spraying (SPPS) [15], and high velocity oxygen fuel (HVOF) [16]. The methods of APS and EB-PVD are now widely used for the deposition of TBCs. APS thermal barrier coatings have a relatively low application cost, and are generally less durable than EB-PVD TBCs [17,18].

Previous studies have showed that the growth of thermally grown oxide and thermal expansion coefficient mismatch between metallic substrate and ceramic top coat during the thermal cycling were the two main factors that limited the

*Corresponding author. Tel.: +98 31 2522 5041; fax: +98 31 2522 8530.
E-mail addresses: r_ghasemi@mut-es.ac.ir, reza.ghasemi65@gmail.com (R. Ghasemi).

0272-8842/$ - see front matter © 2013 Elsevier Ltd and Techna Group S.r.l. All rights reserved.
http://dx.doi.org/10.1016/j.ceramint.2013.06.008

lifetime of thermal barrier coatings [19,20]. Compared to the conventional TBCs, the nanostructured TBCs possess a relatively better thermal shock resistance due to bimodal microstructure container of nano-zones and the existence of an extra source of porosity associated with the nano-zones [21,22]. However, the thermal shock resistance of the nanostructured TBCs should be improved extensively in order for them to be used in industry. Laser glazing is a promising process for proving the thermal shock resistance of the TBCs [23,24]. Laser glazing provides remelting and succeeding solidification of the surface, resulting in a dense top layer with a network of continuous cracks perpendicular to the surface [25,26]. Previous studies showed that the segmented cracks produced by laser glazing were found to improve the strain accommodation, finally leading to the improvement of thermal shock lifetime extension of TBCs, in comparison with plasma-sprayed TBCs [23,24].

In recent years, much research has been conducted on laser glazing of YSZ thermal barrier coatings; however, the as-sprayed YSZ thermal barrier coatings used for laser glazing were mainly prepared using conventional YSZ starting powder. Therefore, the interest is in laser glazing of the YSZ thermal barrier coatings by using the nanostructured YSZ agglomerated powders to effectively improve the performance of the TBCs.

2. Materials and methods

2.1. Materials

A well-polished and cleaned Inconel 738LC Ni-based superalloy was used as the substrate material. An Ni–22Cr–10Al–1.0Y (wt%) type metallic powder (AMDRY 962, Sulzer Metco Inc., USA) was used for spraying the bond coat of TBCs. The spherical powders were gas atomized and the particles size was 56–106 μm, as shown in Fig. 1(a). Commercially obtained spray-dried yttria stabilized zirconia powders (ZrO_2–7 wt% Y_2O_3, Nanox S4007, Inframet Corp., Farmington, CT) containing nanoscale submicrostructure were used as feedstock to deposit the top coat. Fig. 1(b) shows the FESEM image of the nanostructured YSZ agglomerated powders. It can be seen that the powders were spherical and the size distribution of particles was mainly in the range of 15–150 μm. The transmission electron microscopy (TEM) morphology of the grains in the nanostructured YSZ powder is shown in Fig. 1(c). X-ray diffraction results (Fig. 2) showed that the nanostructured YSZ agglomerated powder mainly consisted of only non-transformable tetragonal phase. From the broadening of the X-ray peaks, the average crystallite size was calculated using the Scherrer equation. The average crystallite size estimated from Scherrer equation was 34 nm. As such it was in excellent agreement with TEM results (Fig. 1(c)).

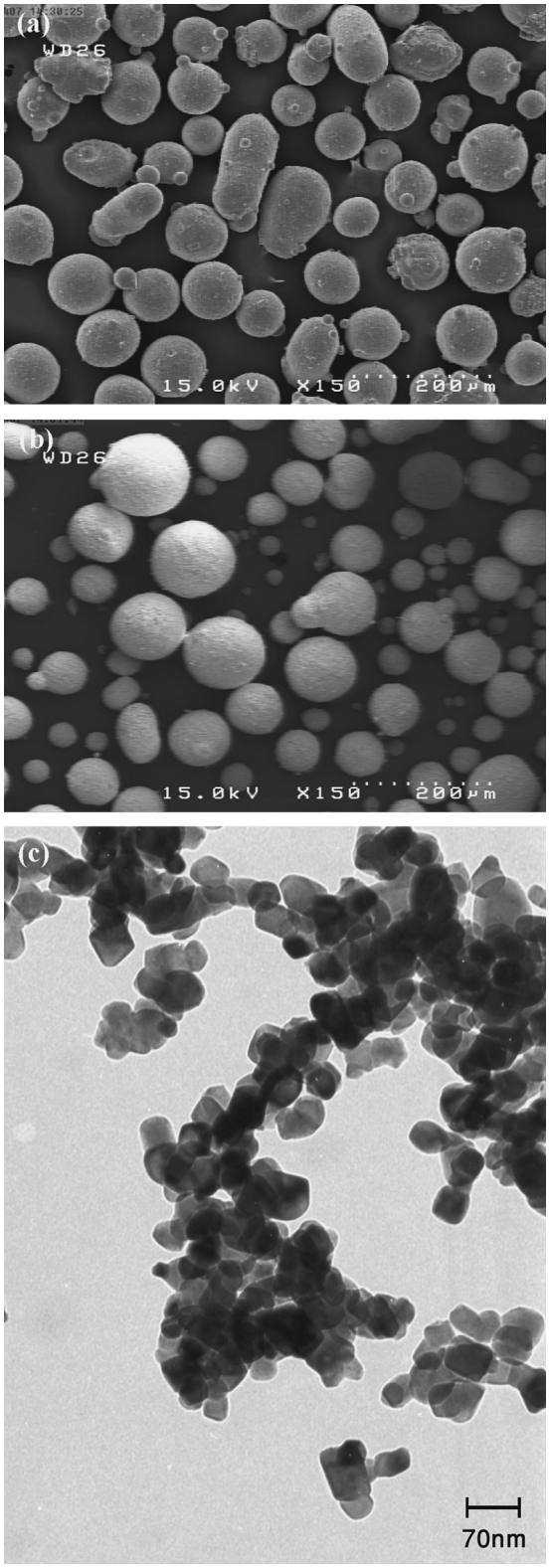

Fig. 1. FESEM micrographs of starting powder: (a) NiCrAlY powder, (b) agglomerated nanostructured YSZ powder and (C) the TEM grain morphology of the nanostructured YSZ powder.

2.2. Air plasma spraying

The thermal barrier coatings, composed of a bond coat (180 ± 25 μm thick) and a top coat (265 ± 25 μm), were fabricated by a Metco A3000S air plasma spray system using Sulzer-Metco F4-MB plasma gun (Sulzer Metco AG, Switzerland). The feedstock powders were fed with Twin-system 10-C. Before the deposition of the bond coat layer, the substrate

surface was grit-blasted with alumina abrasive powder of 24 mesh, at 5 bar, 90° blasting incidence angle and a blasting distance of 10 cm. After grit-blasting, surface roughness was approximately 7.13 μm. During spraying, the substrate and coatings were cooled using the compressed air. Spray conditions of the bond coat and the ceramic layer are listed in Table 1.

2.3. Laser glazing

After APS process, YSZ top coat was post-treated by an Nd: YAG pulsed laser model PIM3475, with the wavelength of 1.064 μm, mean power of 750 W and standard square shaped pulses. The laser was operated in multimode laser oscillation. It could be pulsed at repetition rates ranging from 1 Hz up to 250 Hz. Before performing the laser treatment, power was measured by a powermeter (500 W-Lp Ophir). The system was also equipped with an X–Y table for accurate movement of the specimens. In order to cover the coating surface completely, the specimens were subjected to multiple scans with an overlap of 20% between consecutive tracks, always in the same direction. Laser glazing processing parameters are illustrated in detail in Table 2.

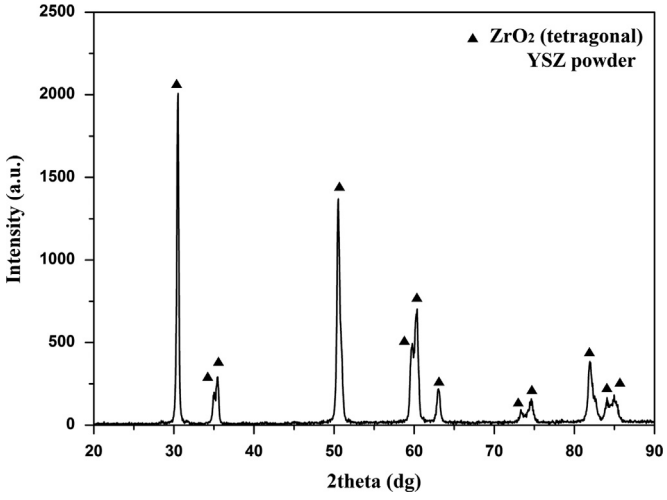

Fig. 2. XRD patterns of agglomerated nanostructured YSZ powder.

2.4. Thermal shock test

The thermal shock test of both plasma-sprayed and laser-glazed coatings was carried out by heating and water quenching method. Each cycle consisted of 15 min holding specimens in the furnace at 1000 °C, followed by direct quenching into water. When a TBC spallation area reached to about 20% of the surface of the top coat, the test was stopped and the number of thermal shock cycles for each specimen was recorded. After every five cycles, the weights of the specimens were measured. Three specimens were tested to obtain the average value of thermal shock lifetime of the coating.

2.5. Specimens characterization

The morphology of the nanostructured YSZ powder was investigated by transmission electron microscopy (TEM; CM 200 FEG, Philips, Netherlands). Morphology powder and coating microstructures were characterized by scanning electron microscopy (SEM; VEGA\\ TESCAN, Czech Republic) and field emission electron microscopy (FESEM; S-4160, Hitachi, Japan). Energy dispersive spectroscopy (EDS; SAMX, VEGA\\ TESCAN, Czech Republic) was used in elemental analysis in SEM studies. Phase identification of powders and coatings was carried out by an X-ray diffraction XRD (D8 ADVANCE, Bruker, Germany) using Cu kα radiation ($\lambda = 0.15406$ nm) produced at 40 kV and 40 mA. The analyzed range of the diffraction angle 2θ was between 20° and 90°, by step width of 0.03°, and a time per step equal to 1 s. The surface roughness (*Ra*) of YSZ coating was measured by a Mitutoyo Surftest profilometer (Mitutoyo SJ-201 P, Japan) with a cut-off length of 800 μm and a measurement length of 4 mm. The roughness reported was the average of five values scanned from different areas on the coating surface.

3. Results and discussion

3.1. Coatings feature

Fig. 3(a) shows the surface morphology of as-sprayed coating. Initial assessment of the image reveals that the coating consists of two kinds of microstructures. One is the smooth and dense phase that results from the well-molten state of

Table 1
Parameters of plasma spraying.

Parameter	NiCrAlY	Nanostructured YSZ
Current (A)	600	600
Voltage (V)	75	72
Primary gas, Ar (SLPM[a])	65	35
Secondary gas, H_2 (SLPM)	14	10
Carrier gas, Ar (SLPM)	2.3	3.5
Powder feed rate (g/min)	40	18
Spray distance (mm)	120	120

[a]Standard liter per minute.

Table 2
Laser glazing parameters.

Parameter	Value
Average working power (W)	82
Pulsed frequency (Hz)	38
Pulse width (ms)	1.2
Scanning speed (mm/s)	10
Overlap (mm)	0.2
Distance (mm)	10

particles, while the other one contains porous and rough phases, indicating non-molten or semi-molten state of particles [27,28]. The surface of coating was very rough and its surface roughness (*Ra*) was about 9.20 μm, due to partially molten particles involved in lower deformation impact of the surface as compared to fully molten particles. In addition, as shown in Fig. 3(a), microcrack was formed after the relaxation of the residual stresses when the coating was cooled. It relates to the increase of the roughness of the as-sprayed coating [29,30]. Fig. 3(b) shows the non-melted and partially molten zone of Fig. 3(a) at a higher magnification. After laser glazing, surface of coating showed a complete resolidification; network segmented cracks perpendicular to the surface can also be seen from Fig. 3(c). These remelting and resolidification phenomena resulted in the reduction of surface roughness ($Ra = 2.58$ μm) [31,32]. Cracking is due to shrinkage and thermal stresses produced during rapid solidification [33,34].

Fig. 4(a) shows the fracture surface of as-sprayed nanostructured coating. These images show that microstructure features of nanostructured as-sprayed coating consist of nanosized zone that resulted from non-molten and partially molten part of starting powder, and microcolumnar grains formed from the resolidification of the molten part, pores and cracks due to the residual stresses during the deposition process [28,35,36]. Fig. 4(b) shows the initial nanostructure of powder retains in the coating. Fig. 4(c) shows the fracture cross section of the laser glazed coating. Measured thickness of the glazed layer was 23–28 μm and segmented crack extended throughout the remelted layer thickness. The principal features in the plasma-sprayed nanostructured coating were all vanished after lase glazing. It can be seen from Fig. 4(c) that the microstructure of laser-glazed coating can be altered from single columnar grains to a combination of equiaxed grains on the surface and columnar grains in the fracture cross section [26,37].

X-ray analysis of plasma-sprayed and laser-glazed coatings (Fig. 5) clearly showed that only the non-transformable phase (T') was present. The formation of this phase is due to the rapid solidification during the process of APS and laser glazing [34,38]. The cooling rate of the splats during plasma spraying and laser glazing was estimated to be 10^7 °C/s and 10^3–10^4 °C/s, respectively [24]. It can be seen from Fig. 5 that there are no new phases in the as-glazed coating as compared to the as-sprayed coating. Therefore, laser glazing has no effect on the phase transformation of TBC. The relative intensity of the individual diffraction peaks was greatly changed due to the glazing process. This is due to the change of microstructure.

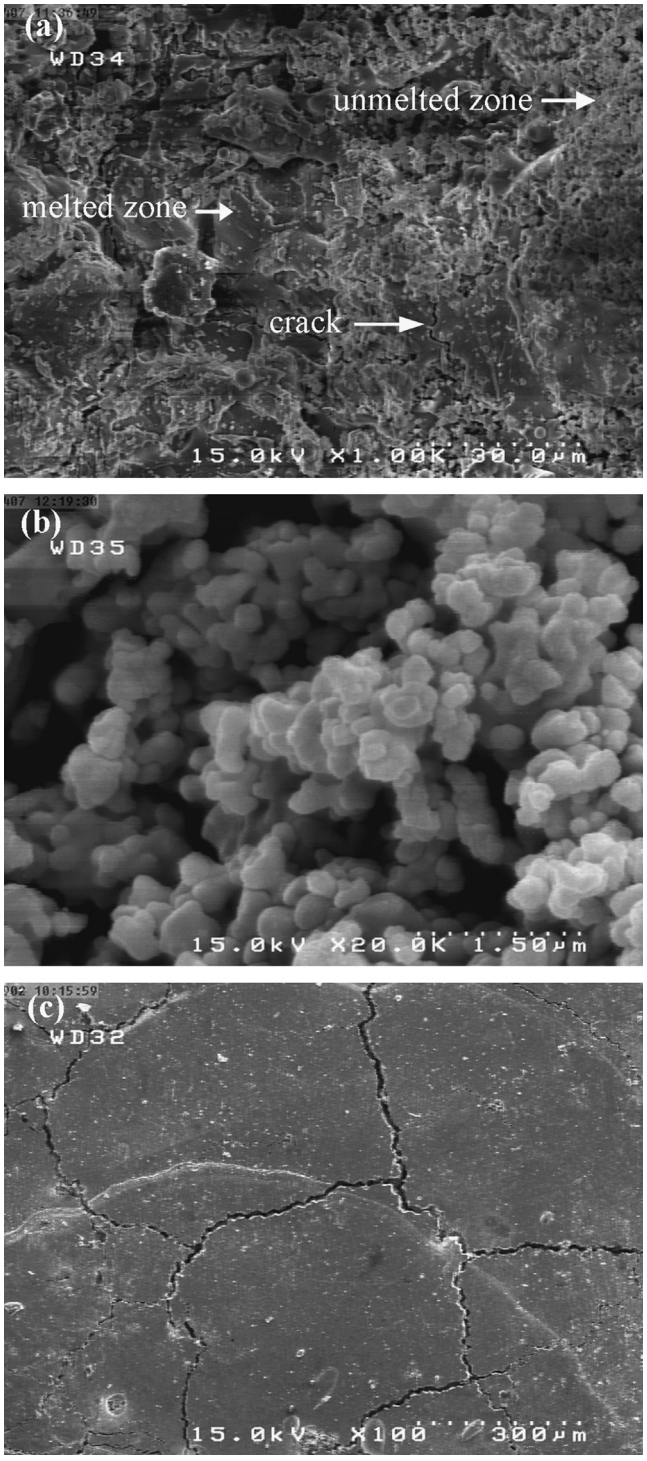

Fig. 3. FESEM micrographs of: (a) top surface of the plasma-sprayed nanostructured coating (b) partially melted zone of (a) at a higher magnification and (c) top surface of the laser-glazed coating.

Increasing relative intensity peak in the laser-glazed coating is due to the columnar grain orientation, which is caused by the laser glazing process [34,39].

3.2. Thermal shock behavior

Fig. 6 shows the macroscopic image of plasma-sprayed and laser-glazed coatings during thermal shock test. It can be seen

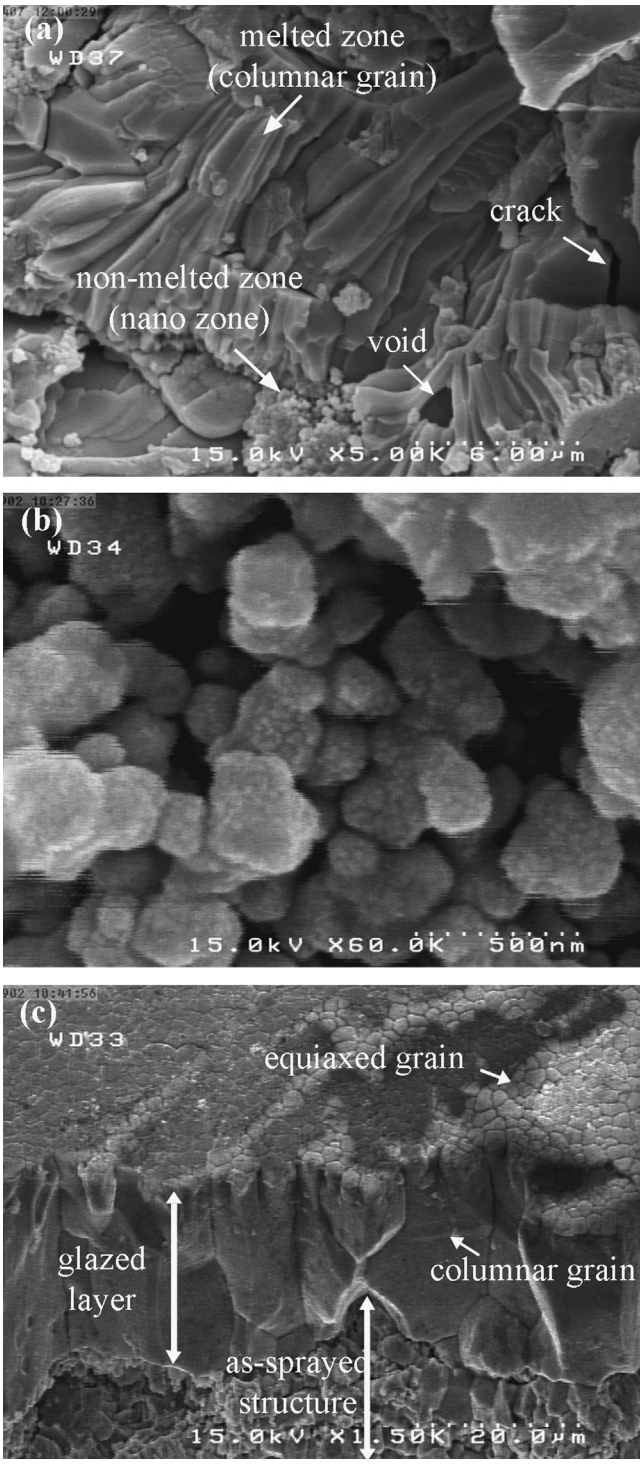

Fig. 4. FESEM micrographs of (a) fractured cross-section of the plasma-sprayed nanostructured coating (b) non-molten nanoparticles within coating at a high magnification and (c) fractured cross-section of the laser-glazed coating.

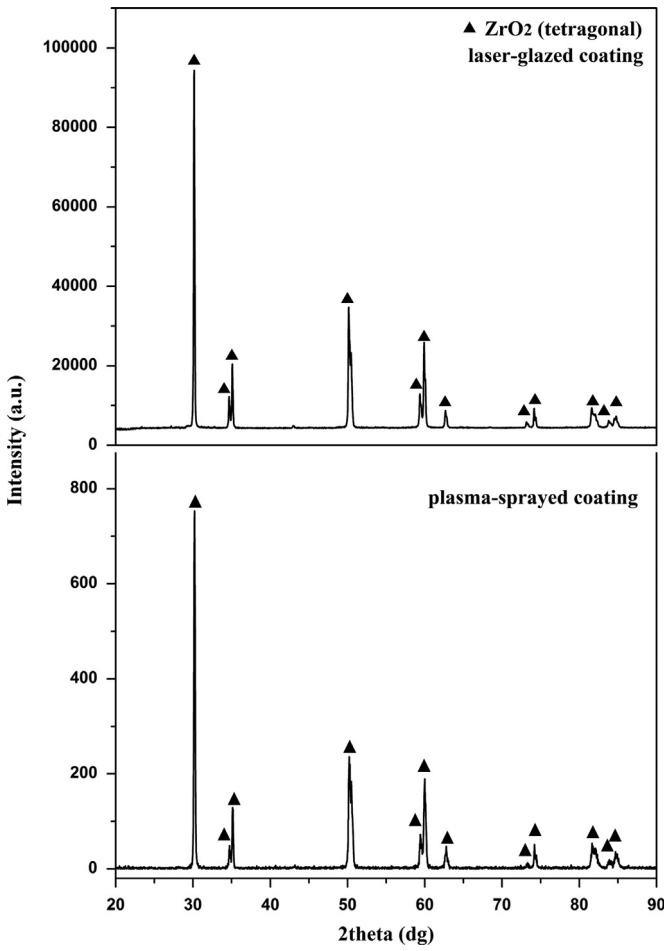

Fig. 5. XRD patterns of as-sprayed and laser-glazed nanostructured YSZ coating.

that failure in both coatings was initiated from the brim and then propagated to the adjacent area. Starting failure from the brim is due to singularity of thermal stresses at the brim. Other studies [21,23,40] have also pointed the edge effects on failure during the thermal cycling. So the failure of coatings is initiated firstly in the relatively high stress area associated with the geometry of the specimens such as brim of samples.

Fig. 7 shows the weight change versus the number of cycles during thermal shock test. Both the plasma-sprayed and laser-glazed coatings initially gained weight due to oxidation of substrate free surface and bond coat and then lost weight due to delamination and spallation of the YSZ top coat. Sudden weight loss of as-sprayed coating expression showed that coating spallation had occurred, while the gradual weight loss of as-glazed coating showed that coating delamination had occurred [21,23].

Fig. 8 shows the fractured cross-section of the plasma-sprayed and laser-glazed coatings after thermal shock test. The failure in the YSZ top coat was propagated mainly by horizontal cracks linked up by propagation through dense YSZ. From the fracture cross-section micrographs, there appears to be two different failure mechanisms occurring with these coatings. The first failure mechanism occurred in the plasma-sprayed coatings. It is characterized by failure associated with cracking and spallation of the TBC well within the YSZ top coat and away from the interface between the bond coat and top coat. This is a typical failure mechanism of plasma-sprayed TBCs caused by thermal stresses arising from the different thermal expansion between the ceramic top coat and the metallic bond coat [41,42]. Failure mechanism usually

Fig. 6. Macroscopic image of: (a) plasma-sprayed and (b) laser-glazed samples during thermal shock testing.

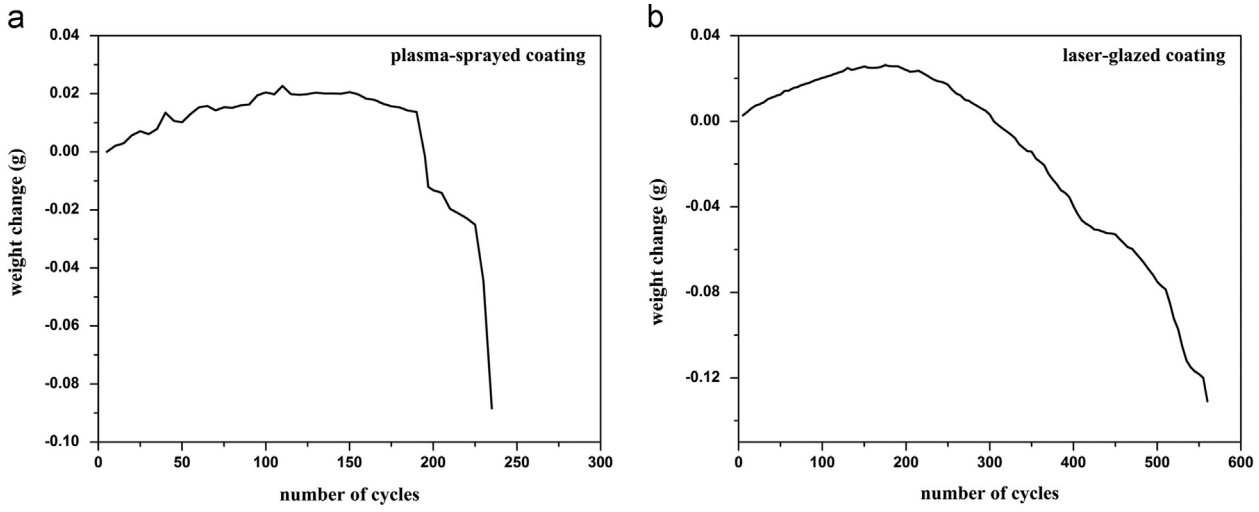

Fig. 7. Weight change as a function of cycle number for plasma-sprayed and laser-glazed samples.

leads to failure after a relatively short number of cycles. It is so short that the effects of bond coat oxidation have not yet become important (246 cycles). The second failure mechanism is associated with the laser-glazed coating. Here failure occurs at or very near the top coat-TGO interface and it is associated with bond coat oxidation affects. This failure mechanism occurs after an increased number of cycles (563 cycles), allowing for bond coat oxidation to occur [43,44].

Fig. 9 shows a higher magnification of the fracture cross-section of the laser glazed coating shown in Fig. 8(b). It is evident that a TGO layer was formed on the bond coat and some horizontal cracks were developed in the YSZ top coat to the TGO. Fig. 10 shows the EDS analysis of top coat-bond coat interface (A and B points in Fig. 8) for both as-sprayed and laser-glazed samples. According to SEM micrograph and EDS analysis, TGO (Al reach area) was not formed for plasma-sprayed coating, while in laser-glazed coating, it was formed.

The second mechanism, formation of the TGO at the interface between the top coat and bond coat, caused the localized expansion which exerted additional tension on the YSZ surrounding the TGO. When the intensity of the tension exceeded the cohesive strength of the YSZ lamellar, the crack was propagated into the YSZ top coat closing the TGO layer. This may cause the failure of YSZ from the TGO [42–44].

Fig. 11 presents the XRD patterns of failed plasma-sprayed and laser-glazed coatings. Results of XRD patterns showed that the as-sprayed and laser-glazed coatings consisted of non-transformable tetragonal phase (T′) of zirconia with a very small amount of calcium zirconium oxide ($CaZrO_3$). The formation of $CaZrO_3$ was due to calcium in the tap water that reacted with zirconium during the test [45,46]. The XRD analysis results indicated that the T′ phase was not decomposed into monoclinic phase (m) under thermal shock test. The phase transformation of T′ to m is associated with a volume

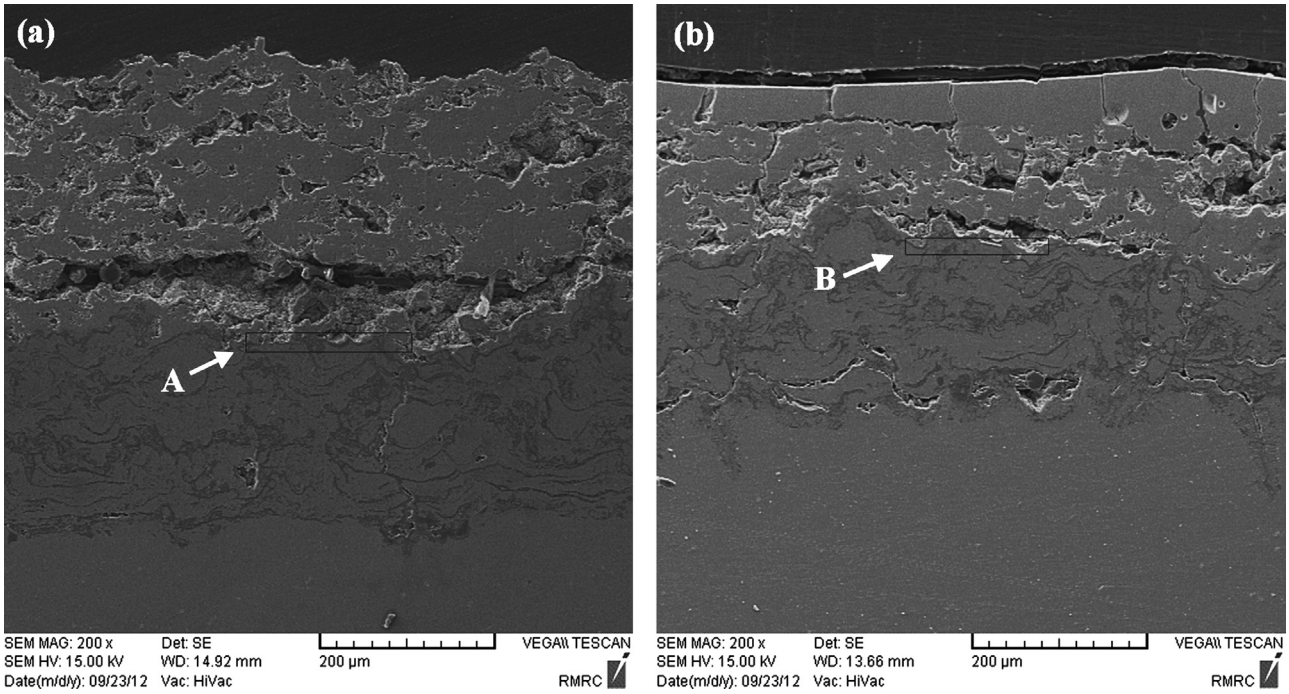

Fig. 8. SEM micrographs of cross-section of: (a) plasma-sprayed and (b) laser-glazed coatings after thermal shock testing.

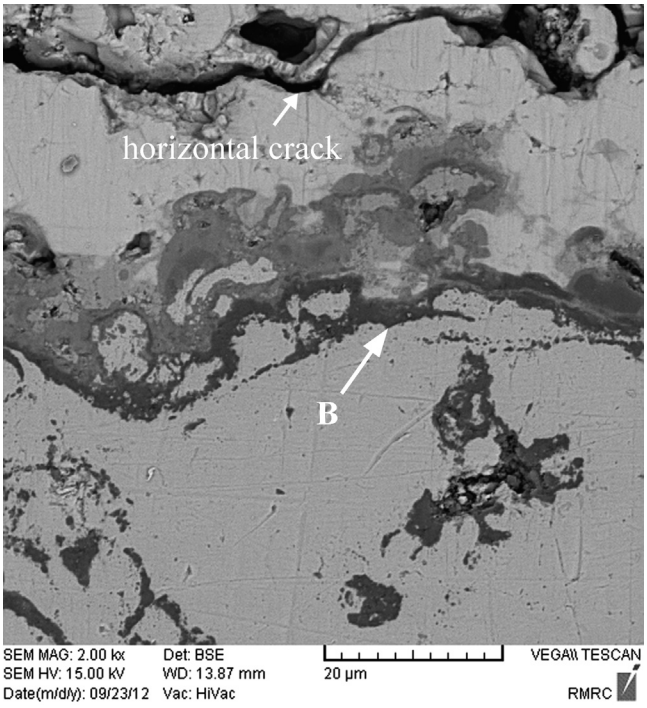

Fig. 9. SEM micrographs of cross-section of laser-glazed coatings at a high magnification after thermal shock testing.

Expansion of up to 5%. The volume expansion deteriorates the integrity of YSZ top coat and causes the failure of TBCs. Anyway, in this work, no phase transformation was observed during the thermal shock test. Accordingly, stresses resulting from phase transformation had no effect on both coatings failure [3,47].

It can be seen from Fig. 7 that the laser-glazed coating exhibited 2.5 improvement in lifetimes, relative to the plasma-sprayed coating. The higher thermal shock resistance of the laser-glazed coatings, as compared to the plasma-sprayed coatings, can be attributed to the coating microstructure. Microstructure of plasma-sprayed coting consisted of rough surface to form a splat and lamellar microstructure in the fracture cross-section, while after laser glazing, the surface of coating showed complete resolidification with network segmented cracks, which were perpendicular to the surface, and columnar grain in the fracture surface [25,26,28,32]. The segmented cracks induced by laser glazing accommodated thermal stress that arose from the mismatch in thermal expansion between the top cat and the bond coat [23,24,37]. Columnar grain microstructure in the fracture cross-section of laser-glazed coating allowed the lateral expansion and contraction during the heating and cooling process. So this microstructure had the capacity for a high degree of expansion and decreased the thermal stress resulting from the mismatch in the thermal expansion coefficient between the ceramic top coat and the metallic substrate [37,48].

4. Conclusion

In this study, microstructure and thermal shock behavior of plasma-sprayed and laser-glazed TBC were investigated; some important results can be summarized as follows:

(1) The nanostructured as-sprayed coting possessed a lamellar structure consisting of nanosized particles and microcolumnar grains, while laser-glazed coating contained a columnar grain in the fracture and an equiaxed grain on the surface.

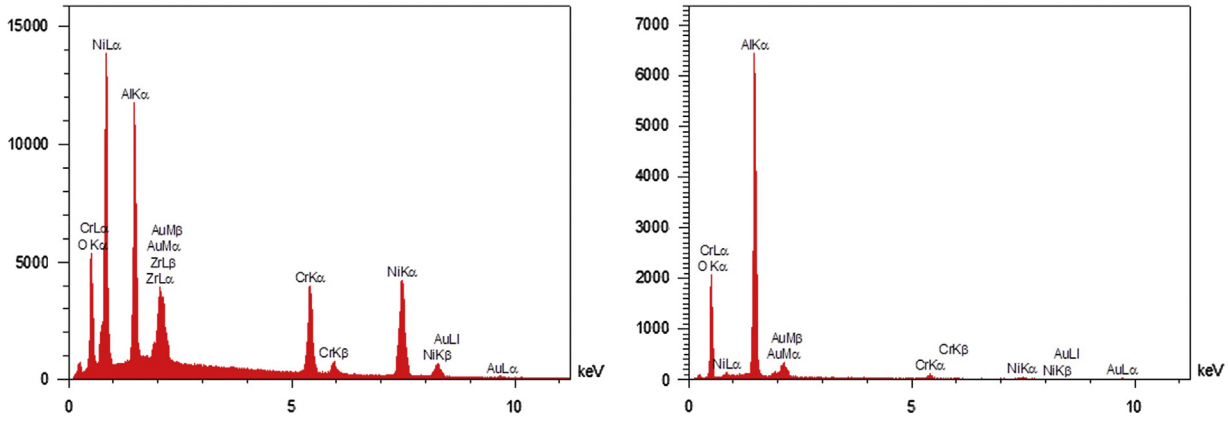

Fig. 10. EDS analysis of: (a) A and (b) B points shown in Fig. 8.

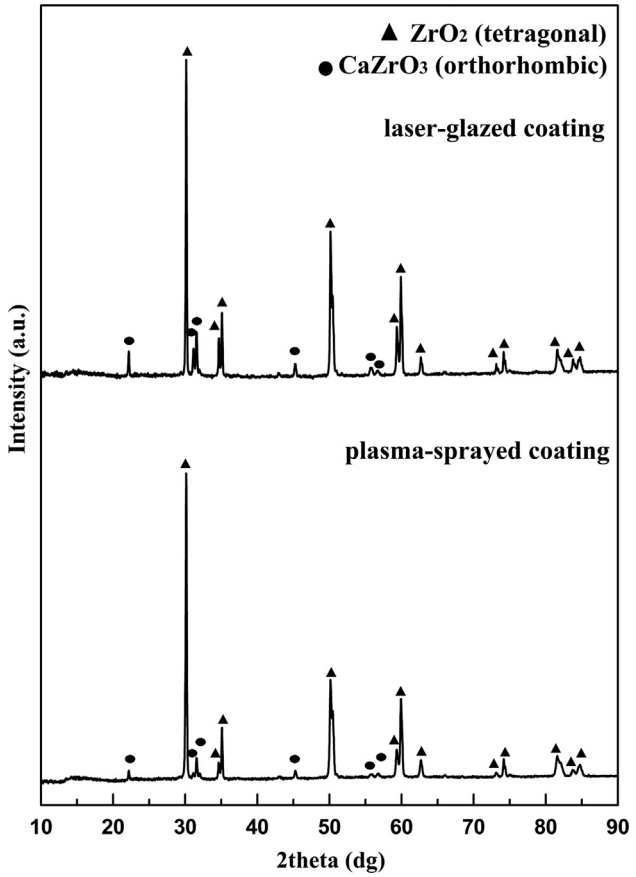

Fig. 11. XRD patterns of: (a) plasma-sprayed and (b) laser-glazed coatings after thermal shock testing.

(2) Both as-sprayed and laser-glazed coatings consisted of tetragonal phase (T′) and failure of these coatings after thermal shock test did not cause phase instability of YSZ top coat.
(3) Laser-glazed TBCs had a thermal shock resistance higher than that of plasma-sprayed TBCs due to change of microstructure.
(4) The network segmented cracks perpendicular to the surface and columnar grain in the fracture surface were all helpful in accommodating thermal stress of as-glazed coating.

Acknowledgments

This work was supported by the Malek-Ashtar University of Technology, Department of Materials Engineering. The authors would like to gratefully appreciate the contribution of Morteza Hajizadeh Oghaz and Mehdi Naderi.

References

[1] M. Abbas, H. Guo, M.R. Shahid, Comparative study on effect of oxide thickness on stress distribution of traditional and nanostructured zirconia coating systems, Ceramics International 39 (2013) 475–481.
[2] C.S. Ramachandran, V. Balasubramanian, P.V. Ananthapadmanabhan, Erosion of atmospheric plasma sprayed rare earth oxide coatings under air suspended corundum particles, Ceramics International 39 (2013) 649–672.
[3] R. Ahmadi-Pidani, R. Shoja-Razavi, R. Mozafarinia, H. Jamali, Evaluation of hot corrosion behavior of plasma sprayed ceria and yttria stabilized zirconia thermal barrier coatings in the presence of Na_2SO_4+V_2O_5 molten salt, Ceramics International 38 (2012) 6613–6620.
[4] S. Das, S. Datta, D. Basu, G.C. Das, Glass–ceramics as oxidation resistant bond coat in thermal barrier coating system, Ceramics International 35 (2009) 1403–1406.
[5] C.R.C. Lima, N. Cinca, J.M. Guilemany, Study of the high temperature oxidation performance of thermal barrier coatings with HVOF sprayed bond coat and incorporating a PVD ceramic interlayer, Ceramics International 38 (2012) 6423–6429.
[6] H.J. Huang, M.C. Wang, The phase formation and stability of tetragonal ZrO_2 prepared in a silica bath, Ceramics International 39 (2013) 1729–1739.
[7] G. Di Girolamo, F. Marra, C. Blasi, E. Serra, T. Valente, Microstructure, mechanical properties and thermal shock resistance of plasma sprayed nanostructured zirconia coatings, Ceramics International 37 (2011) 2711–2717.
[8] N. Wang, C. Zhou, S. Gong, H. Xu, Heat treatment of nanostructured thermal barrier coating, Ceramics International 33 (2007) 1075–1081.
[9] Y. Bai, L. Zhao, J.J. Tang, S.Q. Ma, C.H. Ding, J.F. Yang, L. Yu, Z.H. Han, Influence of original powders on the microstructure and properties of thermal barrier coatings deposited by supersonic atmospheric plasma spraying, part II: properties, Ceramics International 39 (2013) 4437–4448.
[10] Y. Li, Y. Xie, L. huang, X. Liu, X. Zheng, Effect of physical vapor deposited Al_2O_3 film on TGO growth in YSZ/CoNiCrAlY coatings, Ceramics International 38 (2012) 5113–5121.
[11] C. Chen, H. Guo, S. Gong, X. Zhao, P. Xiao, Sintering of electron beam physical vapor deposited thermal barrier coatings under flame shock, Ceramics International 39 (2013) 5093–5102.

[12] S. Guo, Y. Kagawa, Isothermal and cycle properties of EB-PVD yttria-partially-stabilized zirconia thermal barrier coatings at 1150 and 1300 °C, Ceramics International 33 (2007) 373–378.
[13] J.R.V. Garcial, T. Goto, Thermal barrier coatings produced by chemical vapor deposition, Science and Technology of Advanced Materials 4 (2003) 397–402.
[14] F. Tarasi, M. Medraj, A. Dolatabadi, J.O. Berghaus, C. Moreau, Phase formation and transformation in alumina/YSZ nanocomposite coating deposited by suspension plasma spray process, Journal of Thermal Spray Technology 19 (2010) 787–795.
[15] A. Jadhav, N.P. Padture, F. Wu, E.H. Jordan, M. Gell, Thick ceramic thermat barrier coatings with high durability deposited using solution-precursor plasma spray, Materials Science and Engineering A 405 (2005) 313–320.
[16] T.A. Dobbins, R. Knight, M.J. Mayo, HVOF thermal spray deposited Y_2O_3-stabilized ZrO_2 coatings for thermal barrier applications, Journal of Thermal Spray Technology 12 (2003) 214–225.
[17] S. Guo, Y. Kagawa, Effect of thermal exposure on hardness and Young's modulus of EB-PVD yttria-partially-stabilized zirconia thermal barrier coatings, Ceramics International 32 (2006) 263–270.
[18] Y. Bai, J.J. Tang, Y.M. Qu, S.Q. Ma, C.H. Ding, J.F. Yang, L. Yu, Z.H. Han, Influence of original powders on the microstructure and properties of thermal barrier coatings deposited by supersonic atmospheric plasma spraying, part I: microstructure, Ceramics International 39 (2013) 5113–5124.
[19] B. Liang, Chuanxian Ding, Thermal shock resistances of nanostructured and conventional zirconia coatings deposited by atmospheric plasma spraying, Surface and Coatings Technology 197 (2005) 185–192.
[20] C. Zhou, N. Wang, H. Xu, Comparison of thermal cycling behavior of plasma-sprayed nanostructured and traditional thermal barrier coatings, Materials Science and Engineering A 452–453 (2007) 569–574.
[21] H. Jamali, R. Mozafarinia, R. Shoja-Razavi, R. Ahmadi-Pidani, Comparison of thermal shock resistances of plasma-sprayed nanostructured and conventional yttria stabilized zirconia thermal barrier coatings, Ceramics International 38 (2012) 6705–6712.
[22] C. Zhou, Q. Zhang, Y. Li, Thermal shock behavior of nanostructured and microstructured thermal barrier coatings on a Fe-based alloy, Surface and Coatings Technology 217 (2013) 70–75.
[23] R. Ahmadi-Pidani, R. Shoja-Razavi, R. Mozafarinia, H. Jamali, Improving the thermal shock resistance of plasma sprayed CYSZ thermal barrier coatings by laser surface modification, Optics and Lasers in Engineering 50 (2012) 780–786.
[24] J.H. Lee, P.C. Tsai, C.L. Chang, Microstructure and thermal cyclic performance of laser-glazed plasma-sprayed ceria–yttria-stabilized zirconia thermal barrier coatings, Surface and Coatings Technology 202 (2008) 5607–5612.
[25] R. Ahmadi-Pidani, R. Shoja-Razavi, R. Mozafarinia, H. Jamali, Laser surface modification of plasma sprayed CYSZ thermal barrier coatings, Ceramics International 39 (2013) 2473–2480.
[26] R. Ghasemi, R. Shoja-Razavi, R. Mozafarinia, H. Jamali, Laser glazing of plasma-sprayed nanostructured yttria stabilized zirconia thermal barrier coatings, Ceramics International http://dx.doi.org/10.1016/j.ceramint.2013.05.066 in press.
[27] H. Jamali, R. Mozafarinia, R. Shoja-Razavi, R. Ahmadi-Pidani, M.R. Loghman-Estarki, Fabrication and evaluation of plasma-sprayed nanostructured and conventional YSZ thermal barrier coatings, Current Nanoscience 8 (2012) 402–409.
[28] R. Ghasemi, R. Shoja-Razavi, R. Mozafarinia, H. Jamali, Comparison of microstructure and mechanical properties of plasma-sprayed nanostructured and conventional yttria stabilized zirconia thermal barrier coatings, Ceramics International http://dx.doi.org/10.1016/j.ceramint.2013.04.068 in press.
[29] R. Ahmadi-Pidani, R. Shoja-Razavi, R. Mozafarinia., H. Jamali, Comparison of hot corrosion resistance of YSZ and CYSZ thermal barrier coatings in presence of sulfate-vanadate molten salts, Advanced Materials Research 472–475 (2012) 141–144.
[30] D. Seo, K. Ogawa, T. Shoji, S. Murata, Effect of particle size distribution on isothermal oxidation characteristics of plasma sprayed CoNi- and CoCrAlY coatings, Journal of Thermal Spray Technology 16 (2007) 954–966.
[31] M.F. Morks, C.C. Berndt, Y. Durandet, M. Brandt, J. Wang, Microscopic observation of laser glazed yttria-stabilized zirconia coatings, Applied Surface Science 256 (2010) 6213–6218.
[32] C. Zhu, P. Li, A. Javed, G.Y. Liang, P. Xiao, An investigation on the microstructure and oxidation behavior of laser remelted air plasma sprayed thermal barrier coatings, Surface and Coatings Technology 206 (2012) 3739–3746.
[33] A. Petitbon, L. Boquet, D. Delsart, Laser surface sealing and strengthening of zirconia coatings, Surface and Coatings Technology 49 (1991) 57–61.
[34] C. Batista, A. Portinha, R.M. Ribeiro, V. Teixeira, M.F. Costa, C.-R. Oliveira, Surface laser-glazing of plasma-sprayed thermal barrier coatings, Applied Surface Science 247 (2005) 313–319.
[35] W.B. Gong, C.K. Sha, D.Q. Sun a, W.Q. Wang, Microstructures and thermal insulation capability of plasma-sprayed nanostructured ceria stabilized zirconia coatings, Surface and Coatings Technology 201 (2006) 3109–3115.
[36] R.S. Lima, A. Kucuk, C.C. Berndt, Bimodal distribution of mechanical properties on plasma sprayed nanostructured partially stabilized zirconia, Materials Science and Engineering A 327 (2002) 224–232.
[37] H. Chen, Y. Hao, H. Wang, W. Tang, Analysis of the microstructure and thermal shock resistance of laser glazed nanostructured zirconia TBCs, Journal of Thermal Spray Technology 19 (2010) 558–565.
[38] K. Mohammed Jasim, Characterization of laser sealed coatings of yttria partially stabilized zirconia, Optics and Lasers in Engineering 49 (2011) 785–792.
[39] S. Ahmaniemi, J. Tuominen, P. Vuoristo, T. Mantyla, Sealing procedures for thick thermal barrier coatings, Journal of Thermal Spray Technology 11 (2002) 320–332.
[40] H. Jamali, R. Mozafarinia, R. Shoja-Razavi, R. Ahmadi-Pidani, Investigation of thermal shock behavior of plasma-sprayed NiCoCrAlY/YSZ thermal barrier coatings, Advanced Materials Research 472–475 (2012) 246–250.
[41] Y. Wang, H. Guo, S. Gong, Thermal shock resistance and mechanical properties of $La_2Ce_2O_7$ thermal barrier coatings with segmented structure, Ceramics International 35 (2009) 2639–2644.
[42] L. Wang, Y. Wang, X.G. Sun, J.Q. He, Z.Y. Pan, C.H. Wang, Thermal shock behavior of 8YSZ and double-ceramic-layer $La_2Zr_2O_7$/8YSZ thermal barrier coatings fabricated by atmospheric plasma spraying, Ceramics International 38 (2012) 3595–3606.
[43] P.H. Lee, S.Y. Lee, J.Y. Kwon, S.W. Myoung, J.H. Lee, Y.G. Jung, H. Cho, U. Paik, Thermal cycling behavior and interfacial stability in thick thermal barrier coatings, Surface and Coatings Technology 205 (2010) 1250–1255.
[44] S. Das, S. Datta, D. Basu, G.C. Das, Thermal cyclic behavior of glass–ceramic bonded thermal barrier coating on nimonic alloy substrate, Ceramics International 35 (2009) 2123–2129.
[45] A.N. Khan, J. Lu, Behavior of air plasma sprayed thermal barrier coatings, subject to intense thermal cycling, Surface and Coatings Technology 166 (2003) 37–43.
[46] Y. Bai, Z.H. Han, H.Q. Li, C. Xu, Y.L. Xu, Z. Wang, C.H. Ding, J.F. Yang, High performance nanostructured ZrO_2 based thermal barrier coatings deposited by high efficiency supersonic plasma spraying, Applied Surface Science 257 (2011) 7210–7216.
[47] S. Bose, High Temperature Coatings in Connecticut, Elsevier Science and Technology Books, USA, 2007.
[48] U. Schulz, K. Fritscher, A. Ebach-Stahl, Cyclic behavior of EB-PVD thermal barrier coating systems with modified bond coats, Surface and Coatings Technology 203 (2008) 449–455.